Published in final edited form as:

Curr Biol. 2021 January 11; 31(1): 220–227.e5. doi:10.1016/j.cub.2020.10.008.

CLAVATA signaling ensures reproductive development in plants across thermal environments

Daniel S. Jones[1], **Amala John**[1], **Kylie R. VanDerMolen**[1], **Zachary L. Nimchuk**[1,2,3]

[1]Department of Biology, University of North Carolina at Chapel Hill, 250 Bell Tower Dr., Chapel Hill, North Carolina, 27599, USA

[2]Curriculum in Genetics and Molecular Biology, University of North Carolina at Chapel Hill, Chapel Hill, North Carolina, USA

[3]Lead Contact

SUMMARY

The ability to thrive in diverse environments requires that species maintain development and reproduction despite dynamic conditions. Many developmental processes are stabilized through robust signaling pathways which cooperatively ensure proper development [1]. During reproduction, plants like *Arabidopsis thaliana* continuously generate flowers on growing indeterminate inflorescences [2]. Flower primordia initiation and outgrowth depends on the hormone auxin and is robust across diverse environments [3–6]. Here we show that reproductive development under different thermal conditions requires the integration of multiple pathways regulating auxin dependent flower production. In colder/ambient temperatures, the receptor complex CLAVATA2/CORYNE (CLV2/CRN) is necessary for continuous flower outgrowth during inflorescence development. CLV2/CRN signaling is independent of CLAVATA1 (CLV1)-related receptor signaling but involves the CLAVATA3 INSENSTIVE RECEPTOR KINASE (CIK) family co-receptors, with higher order *cik* mutant combinations phenocopying *clv2/crn* flower outgrowth defects. Developing *crn* inflorescences display reduced auxin signaling and restoration of auxin biosynthesis is sufficient to restore flower outgrowth in colder/ambient temperatures. In contrast, at higher temperatures both *clv2/crn* signaling and heat induced auxin biosynthesis via *YUCCA* family genes are synergistically required to maintain flower development. Our work reveals a novel mechanism integrating peptide hormone and auxin signaling in the regulation of flower development across diverse thermal environments.

Graphical Abstract

Correspondence: zackn@email.unc.edu.

AUTHOR CONTRIBUTIONS

D.S.J. designed/performed experiments, analyzed data, acquired funding for support, and wrote the manuscript. A.J. designed/performed experiments and analyzed data. K.R.V performed Col-0 x Ler population experiments. Z.L.N. conceptualized the project and experiments, analyzed data, acquired funding, and wrote the manuscript.

DECLARATION OF INTERESTS

The authors declare no competing interests.

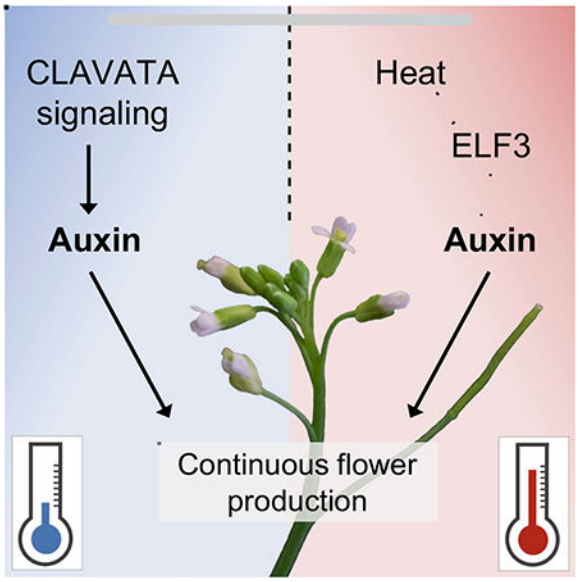

RESULTS AND DISCUSSION

Plants continually develop new organs throughout their life and do so across varied environmental conditions [7]. This indeterminate growth requires balanced cell proliferation and differentiation in stem cell niches, called meristems, at growing apices [8, 9]. During the reproductive phase of *Arabidopsis thaliana*, flower primordia are continuously produced from inflorescence meristems (IM) dependent on the hormone auxin [3–6]. Primordia then proliferate, forming flowers from secondary floral meristems [10, 11]. Cell recruitment into flower primordia is balanced by proliferation in the IM center. The conserved CLAVATA3 (CLV3) peptide signaling pathway dampens stem cell proliferation in shoot and floral meristems [12, 13]. CLV3 signals through a suite of receptors which repress the expression of *WUSCHEL* (*WUS*) in the center of the IM [8, 14]. *WUS* encodes a homeobox transcription factor that positively regulates stem cell proliferation [15]. Among these receptors is the atypical receptor pair CLAVATA2/CORYNE (CLV2/CRN), a leucine rich repeat (LRR) receptor-like protein and a transmembrane pseudokinase, respectively [16–19]. CLV2/CRN negatively regulate IM stem cell proliferation independent of other CLV3 receptors [17, 20]. Here we define a new role for CLV2/CRN in promoting auxin-dependent flower primordia outgrowth and show that signaling through this receptor complex contributes to an environmental buffering mechanism which ensures reproductive developmental stability.

The CLV2/CRN receptor complex promotes flower primordia outgrowth and development

After the production of 1-5 normal flowers in *crn* null mutants (*crn-10*; in the Col-0 ecotype), we noticed a novel phenotype in which flower primordia initiate but fail to develop further and inflorescence internode elongation stalls (Figures 1A–1B; the termination phase). After ~30-40 of these terminated primordia, flower development and inflorescence elongation resumes (recovery phase), indicating that continuous flower production requires *CRN* (Figures 1B and S1A; Video S1). *clv2* null mutants (*rlp10-1*; in Col-0) displayed a

similar phenotype to *crn* (Figure 1C), which was previously observed in *clv2* in a survey of mutants in receptor-like protein genes, but not characterized [21]. To quantify primordia termination, we classified the first 30 attempts to make flowers along the primary inflorescence as normal (complete flowers; formation of all four flower organs [22]), terminated flower primordia (no flower organs develop), or terminated flowers (some flower organs develop, but no gynoecium). *crn* and *clv2* single mutants displayed equivalent defects in flower production (Figure 1E), also observed in *clv2 crn* double mutants, consistent with the documented co-function of CLV2/CRN (Figures 1B–E). *clv2/crn* flower outgrowth defects, and floral meristem size (measured in carpels made per flower), were complemented by expressing fusion proteins from their native promoters (Figure S1B–S1C and S1I–S1J). Using standardized flower primordia staging, we found that *crn* primordia outgrowth deviated from WT (wild type) at flower primordia stage three (FP3), with little proliferation occurring afterwards (Figures 1F–1G; staging as in [23], or stage 2 using Smyth *et. al.* stages [22]). In *crn,* terminated primordia fail to develop floral organs, but occasionally produce bract-like structures, likely due to de-repression of cryptic bract outgrowth (Figure 1H) [24].

Consistent with a role in flower primordia development, *CRN* expression was detected as early as incipient primordia (before primordia outgrowth) and remained throughout primordia formation (Figure 1I). Both CRN (CRN-GFP) and CLV2 (CLV2-Citrine) fusion proteins, expressed by native promoters, confirmed this expression pattern (Figures S1B and S1C). Supporting previous *in situ* results [15], *WUS* expression did not overlap with *CRN* spatially or temporally during primordia specification and outgrowth, when *crn* inflorescence phenotypes diverge from WT (Figures 1I and 1J). The *WUS* domain was expanded in *crn* IMs compared to WT but ectopic *WUS* expression was not detected in terminated *crn* primordia (Figures 1J and 1K) [17]. Additionally, other mutants known to have expanded *WUS* IM expression domains do not display *clv2/crn* primordia outgrowth defects (see below).

CLV2/CRN functions have been studied extensively in the Landsberg-*erecta* (Ler,) background [16, 17, 25]. We found no flower primordia outgrowth defects in null *clv2-1* mutants in Ler, explaining why this phenotype has not been described in this ecotype (Figures S1D–S1E and S1I–S1J). Flower primordia termination was also not observed in *crn-1* (Ler background [17]) or two CRISPR-derived null alleles of *clv2* in Ler (*clv2-10* and *clv2-11;* Figures S1F–S1H and S1I–S1K). F1 plants from an ecotype-hybrid *clv2* null cross of *rlp10-1* (Col-0) X *clv2-1* (Ler) displayed mild termination (Figure S1L). Flower primordia outgrowth defects segregated in a digenic semi-dominant manner in the F2 population (Figure S1M), indicating that dominant modifiers in Col-0 underlie ecotype differences in *clv2/crn* flower outgrowth. Additionally, ecotypic differences were not attributable to the *erecta* (*er*) allele in Ler plants [26], as *clv2 er* double mutants in the Col-0 background had equivalent flower outgrowth defects to *clv2* (Figures S1N–S1P). Double mutants between *CLV2* and the floral identity gene *LEAFY* (*LFY*; *clv2 lfy*) displayed primordia outgrowth defects and *lfy-like* floral organ conversions (Figures S1Q–S1R), indicating that *CLV2/CRN* promote primordia formation independent of *LFY*-floral meristem specification [10, 27]. Collectively, these data show that CLV2/CRN signaling represents a novel ecotype-dependent process regulating primordia outgrowth following reproductive transition.

CLAVATA2/CRN-mediated flower outgrowth requires CIK co-receptors

The CLV2/CRN receptor complex lacks signaling capacity alone, as CRN is a transmembrane pseudokinase [19], suggesting CLV2/CRN require associated functional kinase(s) to signal. CLAVATA candidates with active kinase domains include the CLAVATA3 INSENSTIVE RECEPTOR KINASE1/2/3/4 (CIK1/2/3/4) family co-receptors, CLV1 and the CLV1-related BARELY ANY MERISTEM1/2/3 receptors (BAM1/2/3), which all regulate IM stem cell proliferation [28–31]. CLV1/BAM signals independent of CLV2/CRN in shoot and floral stem cell control [20]. Consistent with this, we found negligible amounts of flower primordia termination in *clv1, bam1/2,* or *bam1/2/3* null mutants (in Col-0) and *crn* was additive in each higher order mutant combination (*crn clv1, crn bam1/2,* and *crn bam1/2/3*; Figures S2A–S2J). CIK1/2/3/4 are leucine-rich repeat (LRR)-II-receptor-like-kinase subfamily co-receptors with overlapping functions with CLAVATA primary receptors, several of which physically interact with CRN [31]. In a previous report we noticed a *crn*-like phenotype in specific *cik* mutant combinations [31]. To confirm this observation, we generated higher order CRISPR null alleles of *CIK1/2/4* in Col-0 (*cik1-3, cik2-3, cik4-3*; Figure S2K). In contrast to *clv1/bam* mutants, *cik1/2/4* displayed flower primordia termination equivalent to *crn* (Figures 2A–2C). Additionally, *cik1/2/4* had enlarged floral meristems quantitatively similar to *crn* (Figure 2D). The protein phosphatase POLTERGEIST (POL), a downstream component of CLAVATA signaling, suppresses *clv2/crn* meristem size defects [17, 32]. *pol* restored flower outgrowth and internode elongation defects in *crn (crn pol;* Figures 2E–2H). Collectively, these data demonstrate that CLV2/CRN signal alongside CIK1/2/4 co-receptors to promote flower outgrowth through a POL-dependent pathway.

CLAVATA receptors respond to CLAVATA3(CLV3)/EMBRYO-SURROUNDING REGION (CLE) peptide ligand(s), and there are 32 *CLEs* in Arabidopsis [33]. CLV3 and a suite of redundant CLE peptides signal via CLV1 to repress IM stem cell proliferation parallel to CLV2/CRN [13, 17, 34, 35]. Flower primordia outgrowth is not impaired in *clv3* or *dodeca-cle* higher order mutants, which combine *clv3* with several redundant *cle* alleles [13], suggesting that additional unknown CLE peptides regulate flower outgrowth through CLV2/CRN/CIK (Figure S2L–S2M). Consistent with this, *crn clv3* double mutants are additive with a clear disruption in flower primordial outgrowth and an enlarged disc-like IM (Figure S2N). The enlarged shoot and fasciated stem of *crn clv3* made quantification of terminated primordia difficult; however, these data support previous work suggesting that CLV2/CRN can act independently of CLV3 [20].

Temperature and *CLV2/CRN* modulate auxin-dependent flower primordia outgrowth

Many developmental programs are robust, ensuring optimal morphology/function across varied conditions [13, 36]. Populations of *A. thaliana* can be found throughout the Northern Hemisphere thriving in diverse environments [7, 37]. Natural variation in traits like flowering time and freezing tolerance are influenced by and/or directly correlated with adaptations to local conditions [7]. While investigating *clv2/crn* we observed remarkable quantitative variability in flower primordia termination at different temperatures. Flower outgrowth defects in *clv2/crn* were suppressed when grown at higher temperatures (31°C) compared to colder/ambient temperatures (16°C/24°C; Figures 3A–3G). Previous work

noted shoot defects in *crn-1* mutants (Ler background) at high temperatures; however, we did not observe this under our conditions (Figures 3H–3I) [17]. Thermomorphogenic pathways regulate high temperature seedling growth by enhancing auxin biosynthesis [38, 39]. At higher temperatures, PHYTOCHROME INTERACTING FACTOR (PIF) family transcriptional regulators activate *YUCCA* (*YUC*) genes, which encode rate-limiting enzymes in auxin biosynthesis [40, 41]. Under colder/ambient temperatures, thermomorphogenesis is negatively regulated by the transcriptional repressor EARLY FLOWERING 3 (ELF3) [42]. As such, *elf3* seedlings display constitutive thermomorphogenic responses and higher auxin production across temperatures. To test if the thermomorphogenesis pathway was sufficient to suppress *clv2/crn* flower outgrowth defects, we generated *crn elf3* double mutants and grew them at colder/ambient temperatures. Consistent with high temperature mediated suppression of *crn,* flower primordia termination was suppressed in *crn elf3* at colder temperatures (Figures 3J–3L). In contrast to the suppression of *crn* primordia outgrowth, *elf3* slightly enhanced carpel numbers compared to *crn* (Figure 3M). This finding supports that CLV2/CRN-mediated outgrowth and CLV2/CRN-mediated meristem size regulation are separable with primordia outgrowth being highly sensitive to thermal conditions. Our data shows that CLV2/CRN/CIK signaling is critical for continuous flower production at colder/ambient temperatures but can be bypassed by thermomorphogenic responses to higher temperatures. As such, while Arabidopsis flower development is robust under various environmental conditions, distinct mechanisms maintain this stability across different temperatures.

To define the mechanisms underlying *crn* primordia termination, we used RNA-seq to identify differentially expressed genes (DEGs) in terminating *crn* IMs compared to WT. Using a strict cutoff (p-value < 0.001), we found 460 DEGs between *crn* and WT IMs, with 236 upregulated and 224 downregulated in *crn* (Figure 4A; Table S1). Enriched Gene Ontology (GO) terms among DEGs included meristem maintenance, flower development, and auxin function (Figure 4B; Table S2) [43–45]. The first two GO term groups are consistent with CRN's role in meristem maintenance [17, 20], and flower development, documented in this study (Tables S1 and S2). The overrepresentation of auxin-associated genes in *crn* IM DEGs (Table S1) is complementary to the thermomorphogenic suppression of *crn*'s primordia termination (Figure 3), suggesting CLV2/CRN regulate auxin function during early flower primordia outgrowth. Therefore, we asked if *clv2/crn* were defective in auxin outputs at lower temperatures and if auxin biosynthesis was required for the high temperature suppression of *clv2/crn*. We visualized the auxin signaling reporter *DR5::GFP* (where GFP positively correlates with increased auxin signaling output) and the auxin perception reporter *DII-Venus* (where Venus negatively correlates with increased auxin perception) in terminating *crn* IMs [46, 47]. There was a significant reduction in DR5::GFP signal in *crn* IMs during termination, specifically in the L1 layer of incipient primordia (Figures 4C–4D and S3A–S3C). Consistently, *DII::Venus* accumulated in the L1 layer of terminated *crn* IMs, a pattern never observed in WT (Figures 4E–4F and S3D). DR5::GFP was restored to WT levels during *crn*'s recovery phase (Figures S3E–S3F). During flower development, the PIN-FORMED1 (PIN1) auxin efflux transporter concentrates auxin to the IM periphery, creating local maxima which trigger flower primordia initiation and subsequent outgrowth [4, 5]. PIN1 reporter levels (PIN1-GFP) [5] were decreased in

terminating *crn* IMs (Figures S3G–S3H); consistent with *PIN1* expression from our RNAseq DEG data. (Table S1). PIN1-GFP levels increased during *crn*'s recovery phase, but not to WT levels (Figure S3I). These data demonstrate an overall reduction in auxin signaling/perception within the IM and developing primordia of *crn* during the termination phase. This decrease is transient and corresponds with flower outgrowth defects, indicating that CLV2/CRN positively regulate auxin dependent flower primordia outgrowth in the IM.

Several auxin biosynthetic genes had decreased expression in *crn* compared to WT, including *YUC* genes that regulate flower development (Figure S3J and Table S3) [48]. To test if low auxin levels contributes to *crn*'s flower outgrowth defects, we expressed *YUC1* in developing primordia of *crn* using the *AINTEGUMENTA* promoter (*ANTp::YUC1*) [6, 49] and grew plants in colder (16-18°C) and ambient (22-24°C) temperatures. At 22-24°C, 9/13 T1 plants suppressed *crn* while only 2/18 plants partially suppressed *crn* at 16-18°C (Figures 4G–4H). This demonstrates that at ambient temperatures (where *crn* terminates), ectopic *YUC1* can suppress flower outgrowth defects; however, the degree of suppression correlates with temperature. Higher order mutant combinations in IM-expressed *YUC1/2/4/6* severely impair floral and vasculature development; however, *yuc1/4* double mutants produce more typical inflorescences with identifiable flowers [48]. We generated *clv2 yuc1/4* triple mutants to reduce YUC-dependent auxin in *clv2* and test whether high temperature suppression of *clv2/crn* flower termination was dependent on *YUC*-mediated auxin biosynthesis. At 16-18°C, *clv2 yuc1/4* triple mutants displayed rates of flower primordia termination comparable to *clv2* (Figure 4I). As such, CLV2/CRN promote auxin mediated primordia outgrowth independent of YUC1/4 in colder temperatures. At 28-31 °C, some *clv2 yuc1/4* triple mutant plants displayed *clv2* flower primordia termination, indicating that at high temperatures YUC1/4 contribute to heat induced suppression (Figure 4J). Surprisingly though, the majority (~60%) of *clv2 yuc1/4* plants had a synergistic response to high temperatures resulting in *pin-like* inflorescences completely lacking flower primordia (Figure 4J). These data suggest that high temperature suppression of *clv2* is dependent on *YUC1/4*-mediated auxin biosynthesis and that under high temperatures, *CLV2/CRN* and *YUC1/4* are synergistically required to maintain flower primordia initiation and outgrowth.

Ensuring robust development and reproduction across environments is a challenge all organisms face. Here we demonstrate that robust flower production in diverse thermal environments is achieved through the synergistic deployment of CLV2/CRN-signaling and ELF3-regulated auxin production via the thermomorphogenesis pathway in Arabidopsis. The relative contribution of each to flower development varies across thermal clines, with CLV2/CRN signaling being critical at colder/ambient temperatures and synergistic with heat-induced auxin production at higher temperatures (Figure S4). Arabidopsis seedlings respond to high temperatures by promoting auxin-dependent hypocotyl elongation, a process negatively regulated by ELF3 [38, 42]. Our work demonstrates that high temperatures and *ELF3* also regulate auxin-dependent primordia production. Interestingly, *clv2 yuc1/4* primordia outgrowth defects were strongly enhanced in warmer conditions. Higher temperatures also enhance penetrance of seedling defects in loss-of-function mutants in the TRANSPORT INHIBITOR RESPONSE1 (TIR)-family auxin receptors [50]. As such, heat might have an unappreciated negative impact on auxin function, with thermomorphogenesis-induced auxin playing a protective role rather than simply directing growth. How

CLV2/CRN stimulate auxin-dependent flower initiation is unknown. Ectopic *YUC1* expression or heat-induced auxin production is sufficient to restore primordia outgrowth to *clv2/crn*. This suggests that CLV2/CRN are not critically required for TIR-dependent auxin perception, ARF5/MONOPEROS dependent transcriptional activity, or the TRYPTOPHAN AMINOTRANSFERASE OF ARABIDOPSIS (TAA1)-mediated conversion of tryptophan to indole-3-pyruvate (IPA) step upstream of YUCCA in auxin biosynthesis [6, 51–53].

clv2/crn defects manifest early in inflorescence development and are transient. Recovery of primordia production is not linked to flower meristem identity or seed/fruit derived auxin production (*clv2 Ify* plants). This suggests that the transition from vegetative to reproductive meristem fate may be sensitized to CLV2/CRN signaling. Nevertheless, *clv2 yuc1/4* plants reveals that CLV2/CRN signaling is required at later steps in inflorescence development as well. Heat stress is known to damage crops in ways that negatively impact yield, including the loss of flower production [54, 55]. As climate change increases global temperatures it will be necessary to mitigate heat impacts on crop yield. If the environmental buffering capacity of CLV2/CRN-signaling is conserved in crop species perhaps it could be deployed to help improve plant responses to climate change.

STAR METHODS

RESOURCE AVAILABILITY

Lead Contact—Information and resource/reagent requests should be directed to and will be fulfilled by the Lead Contact, Zachary Nimchuk (zackn@email.unc.edu).

Materials Availability—Plasmids and Arabidopsis lines made during this study are freely available to academic researchers through the Lead Contact.

Data and Code Availability—Raw RNAseq data described in this study has been deposited into the NCBI Short Read Archive (SRA) database under the BioProject PRJNA661065. Code used to analyze gene expression data can be found on the Nimchuk Lab GitHub page (https://github.com/NimchukLab). All other source data obtained throughout the course of this work have not been deposited to any public repository but are available upon request from the Lead Contact.

EXPERIMENTAL MODEL AND SUBJECT DETAILS

Arabidopsis thaliana accession Columbia (Col-0) was used as our primary model system throughout this work. Some phenotypic comparisons were also made with the accession Landsberg-erecta (Ler), as noted.

Plant growth conditions—Seeds were sterilized and plated on half-strength MS (Murashige-Skoog) media buffered with MES, pH 5.7. Plates were stratified in the dark at 4°C for 2 days and then moved to constant light in a custom-built grow room with environmental control (temperature maintained between 21-25°C), or in a Percival growth chamber (AR-75L3) when growing at a specified temperature. After 7-10 days, seedlings were transplanted to soil (Metro-Mix 360/sand/perlite supplemented with Marathon

pesticide and Peter's 20:20:20 [N:P:K] at recommended levels) and then placed back into the chamber they were germinated in and grown until flowering for phenotypic analysis.

METHOD DETAILS

Plant materials

Mutant alleles used in this study are all in the Col-0 background, unless otherwise noted, and information for each is as follows: *crn* (*crn-10*) [20], *crn-1* in Ler [17], *clv2* in Col-0 (*rlp10-1*) [21], *clv2-1* in Ler [16], *erecta* (*er-105*) [56], *Ify* (*lfy-1*; ABRC CS6228) [27], *clv1* (*clv1-101*) [57], *baml* (*bam1-4*) [30], *bam2* (*bam2-4*) [30], *bam3* (*bam3-2*) [30], *pol* (*pol-6*) [58], *clv3* (*clv3-9*) [30], *dodeca-cle* (*clv3-9*; CRISPR alleles of: *cle9, cle10, cle11, cle12, cle13, cle18, cle19, cle20, cle21, cle22, cle45)* [13], *elf3* (*elf3-1*; ABRC CS3787) [59], *yucl* (SALK_106293) [48], and *yuc4* (SM_3_16128) [48]. Information for previously published transgenic complementation and reporter lines used are as follows: *CRNpro::CRN-GFP* in *crn* [20], *CLV2pro::CLV2-CITRINE* in *clv2* [60], *WUSpro::Ypet-N7* in Col-0 (gift from Paul Tarr – Caltech), *DR5pro::GFP* in Col-0 [61, 62], *DII-Venus* in Col-0 [63], *PIN 1 pro::PIN 1-GFP* in Col-0 [64]. The *DR5pro::GFP, DII-Venus,* and *PIN1pro::PIN1-GFP* lines were all crossed into *crn (crn-10)* for analysis of auxin signaling levels in *crn* shoots compared to WT.

CRISPR mutagenesis of *CIK1/2/4* and *CLV2*

The *pCUT* vector system was used to simultaneously create *cik1, cik2* and *cik4* mutations in the Col-0 background (*cik1-3, cik2-3, cik4-3*), making the *cik1/2/4* higher order mutant [65]. Similarly, the *pCUT* system was used to make multiple unique mutations in *clv2* in the Ler background (*clv2-10, clv2-11*). A *pENTR-D/TOPO* entry vector was modified for golden gate cloning by TOPO cloning in PmeI and BsaI cut sites (*pENTR-GG*). *pENTR-GG* was used to clone tandem cassettes (*cik1/2/4*) or a single cassette (*clv2*) of the U6 promoter, 20 bp guide sequence, and the gRNA scaffold. These guide constructs were then gateway cloned into *pCUT4GTW* vector that expresses Cas9 from the *UBIQUITIN10* promoter. Hygromycin resistant plants were selected in the T1 generation and sequenced to detect editing of the target genes; *CIK1* (AT1G60800), *CIK2* (AT2G23950), and *CIK4* (AT5G45780) or *CLV2* (AT1G65380). To make stable *cik1/2/4*, T2 seed from editing *cik1/2/4* lines were grown for 2 weeks under standard conditions, heat shocked for 12-24 hours at 35°C [66], and screened for stable edits using dCAPS primers designed by the indCAPS webtool (http://indcaps.kieber.cloudapps.unc.edu/) [67]. Cas9 was segregated out of plants that had stable homozygous mutations in *CIK1/2/4*. To make stable *clv2* alleles in Ler, T2 seed, collected from single branches of T1 plants that had the *clv2* carpel phenotype, were grown in a Percival growth chamber at 16°C (see above), screened for stable mutations while segregating Cas9 out prior to phenotypic analysis.

Columbia-0 X Landsberg-erecfa hybrid *clv2* population

Null *clv2* lines in the Col-0 (*r1p10-1*) and Ler (*clv2-1*) backgrounds were crossed to generate a hybrid population with fixed *clv2* mutations. Segregation of flower termination traits was assessed in the F2 generation. Phenotypic ratios were compared to expected values of a single causative locus (1:2:1) and digenic semi-dominant modifiers (7:6:3) using Chi-

squared analysis (Microsoft Excel v.16.40) to determine the underlying genetic complexity of the ecotypic variability of *clv2* termination.

Generation of binary vectors and transgenic lines

New transgenic lines were generated using floral-dip transformation of binary vectors into specified backgrounds [68]. *pWUSpro::Ypet-N7* (gift from Paul Tarr – Caltech; cloning methods as in [69] but with *Ypet-N7*) was transformed directly into *crn* and the transgene was selected on ½ MS plates with Kanamycin. Four independent lines were selected for downstream analysis with the *WUS* expression domain being equivalent across all lines imaged (see imaging methods for data acquisition details). For *pCRNpro::Ypet-N7*, a pENTR-D *Ypet-N7* (2xYpet-N7 fusion) entry vector was recombined by LR reaction into the *pCRNpro::Gateway* binary vector in the *pMOA33* background [20]. For *pANTpro::YUC1*, the 4 kb 5' *ANT* promoter was amplified from genomic DNA, and cloned up stream of a gateway::OCS terminator cassette in the *pCR2.1* shuttle vector, and sequence verified. The resulting *ANTpro::Gateway::OCS* cassette was then mobilized as a Not1 fragment in to the *pMOA33* binary vector backbone as previously described to create *pANTpro::GTW* [30]. The *YUC1* CDS was amplified from Arabidopsis Col-0 cDNA and cloned into the *pENTR-D* topo vector and sequence verified. This vector was then recombined in an LR reaction into *pANTpro::GTW* to create the *pANTpro::YUC1*.

Photography and time-lapse imaging

Unless specified differently below, young inflorescences were staged at similar developmental timepoints and photographed using a Canon EOS Rebel T5 equipped with a Tokina 100mm f/2.8 AT-X M100 AF Pro D macro lens. Images were edited for brightness and contrast using Gimp v2.10.4 (https://www.gimp.org/). Young inflorescences from Col-0, *crn*, *clv2*, *crn clv2*, *cik1/2/4*, *yuc1/4*, and *clv2 yuc1/4* (Figures 1A'–D', 2B, 4E–F, and 4H–I) were imaged using a Zeiss Stemi 2000-C stereo microscope equipped with a Zeiss Axiocam 105-color digital camera and acquired using Zeiss ZEN software. Time-lapse imaging was done using the Lapse-it (http://www.lapseit.com/) app on an iPhone 6 operating iOS 12.3.1. Imaging began with ~3-week-old Col-0 (WT) and *crn* plants growing in our custom-built grow room. A single image was taken every 30 minutes over the course of 10-12 days. The final movie was compiled at 30 frames per sec and exported into iMovie where it was cropped to show only two plants for comparison of early flowering phenotypes.

Confocal microscopy

Live imaging of inflorescence meristems (IMs) was performed as previously reported [20, 70]. We used either an inverted Zeiss 710 (for: propidium iodide (PI) stained Col-0, *crn*, *CRNpro:Ypet-N7*, *WUSpro::Ypet-N7*, *DR5pro::GFP*, *DII-Venus*, and *PIN1pro::PIN1-GFP*) or a Zeiss 880 (for *CRNpro::CRN-GFP* and *CLV2pro::CLV2-CITRINE*) confocal laser scanning microscope equipped with an inverter (setup described in [71]). Young IMs were dissected immediately following floral transition in order to analyze expression patterns and reporter levels at the same developmental stage as *clv2/crn* flower primordia termination. When analyzing reporter status in recovered IMs of *crn*, shoots were dissected at a later timepoint after flower buds were visibly developing again. All IMs were briefly (~5 mins for WT and ~15 mins for *crn*) stained with PI (final concentration of 50μg/mL for WT shoots

and 15μpg/mL for *crn*) on ice and placed into a petri dish with 2% agarose (w/v) and immersed in cold water, ensuring no bubbles formed around the IM [70]. IMs were imaged using a W Plan-APOCHROMAT 40X (NA = 1.0) water dipping objective. Laser excitation and detected emission ranges were as follows: PI only – laser 561nm diode, PI channel 600-750nm; Ypet/Venus markers with PI – 514nm argon laser, Ypet channel 520-581nm, PI channel 655-758nm; GFP markers (on Zeiss 710) with PI – 488nm argon laser, GFP channel 493-556nm, PI channel 598-642nm; GFP on Zeiss 880 with PI – 488nm argon laser, GFP channel (GaAsP detector) 490-550nm, PI channel (GaAsP detector) 565-610nm; Citrine on Zeiss 880 with PI – 514nm argon laser, Citrine channel (GaAsP detector) 519-550nm, PI channel (GaAsP detector) 565-610nm. Whole IMs were imaged as a z-stack series with a step size optimized for three-dimensional reconstruction of data. All images comparing reporter levels in different backgrounds were obtained with identical specifications: *DR5pro::GFP, DII-Venus,* and *PIN1pro::PIN1-GFP* in both WT and *crn* shoots. Live inflorescence micrographs were all post-processed using ZEN (Zeiss) for three-dimensional reconstructions of IMs and Fiji/ImageJ v.2.0.0-rc-69/1.52u (National Institutes of Health) [72] for single scan images as well as axial views of IMs. Channels corresponding to PI staining in *crn* IMs were almost always gamma corrected (0.8) as penetrance of this fluorescent dye in enlarged *crn* shoots was sometimes limited. *DR5pro::GFP* fluorescence quantification comparing WT and *crn* IMs was done as follows using Fiji/ImageJ v.2.0.0-rc-69/1.52u. Z-stacks were rendered as maximum intensity projections of the GFP channel only using data from the entire IM. A region of interest (ROI) was drawn around each of the first 3 developing primordia (identified as the 3 early primordia with the highest GFP intensities). GFP levels were quantified for each ROI, normalized to the final area of each ROI, and then averaged together to obtain a single value for WT and *crn* IMs. DII-Venus quantification was done using Fiji/ImageJ v.2.0.0-rc-69/1.52u. Due to rapid photobleaching of the Venus fluorescent reporter, single scan images were taken in the L1 layer of WT and *crn* IMs prior to z-stack scans and used for direct comparison. The percentage of L1 cells with the Venus reporter were determined across all imaged IMs, with WT IMs never having reporter in this layer.

Whole shoot reconstruction of *crn* during termination (Figure 1H) was done using fixed and cleared tissue, imaging structural autofluorescence (as in [13]). Young *crn* IM were fixed in FAA (2% formaldehyde, 5% acetic acid, 60% ethanol (w/v)) at 4°C overnight and then dehydrated in a graded ethanol series (70%, 80%, 95% and 100%) for 30 minutes each at room temperature. Tissue was then cleared overnight in methyl salicylate (catalog no. M6752; Sigma Aldrich) and placed in a small glass-bottom petri dish (catalog no. P35G-1.5-10-C; MatTek Corporation) and imaged on a Zeiss 710 CLSM using a Plan-APOCHROMAT 10X (NA = 0.45). Autofluorescence was detected using a 488nm argon laser for excitation and combining two channels for emission detection; Channel 1 – 504-597nm and channel 2 – 629-731nm. Data was gathered as a z-stack and three-dimensional reconstruction was done in Nikon NIS-Elements as a shaded render of both channels combined in grayscale.

RNA Sequencing and Data Analysis

Total RNA was isolated using the EZNA Plant RNA kit (Omega Bio-tek) from 45-50 inflorescence meristems for three biological replicates of both Col-0 and *crn* (*crn-10*) plants. RNA was treated with RNase-free DNase (Omega Bio-tek). Approximately 1.5 ug RNA was used as input material for library preparation, using the Stranded mRNA-Seq kit (Kapa Biosystems) at the High-throughput Sequencing Facility at UNC Chapel hill. 50bp paired-end reads were generated on the NovaSeq 6000 sequencer (illumina) with a read depth of 23-35 million reads per biological replicate. Trimmed raw data was aligned to the *A. thaliana* genome (TAIR10.1) using HISAT2 version 2.2.0 [73] and reads were counted using Subread version 1.5.1 [74]. Subsequent analysis was performed on RStudio with reads normalized using EDASeq version 2.22.0 [75] and RUVseq version 1.22.0 (upper quartile normalization) [76] and differentially expressed genes were identified with a p-value <0.001 using EdgeR version 3.33.0 [77]. These top 460 DEGs were used for GO term analysis from Panther [78]. To obtain the average TPM counts of auxin biosynthetic genes, reads were pseudoaligned to the *Arabidopsis* transcriptome (TAIR10 from plants.ensembl.org) using Kallisto version 0.44.0 [79] and quantified with Sleuth version 0.33.0 [80].

QUANTIFICATION AND STATISTICAL ANALYSIS

Quantitative data from all experiments was compiled and analyzed in GraphPad Prism v.8.3.2. We performed at least two biological replicates for each experiment ensuring consistent results (sample sizes indicated in figure legends). For comparisons of flower termination across conditions, genotypes and/or transgenic lines (Figures 1E, 2C, 2G, 3G, 3L, 4G–H, S1I, S2C–D, S2I–J), only % flower primordia termination (as defined in the paper) was compare across samples using a non-parametric Kruskal-Wallis and a Dunn's multiple comparison test correction where significance was defined as p-value < 0.05. For comparisons of carpel number across genotypes (Figures 2D, 2H, 3M, and S1J), 10 consecutive flowers on the primary inflorescence were counted, starting after the recovery phase in *crn, clv2,* and *cik1/2/4* while starting at the 11th flower in genotypes that had no flower primordia termination or partially suppressed flower primordia termination (Col-0, Ler, *clv2-1, crn-1, pol, crn pol, elf3,* and *crn elf3*). Carpel number was compared statistically using a non-parametric Kruskal-Wallis and a Dunn's multiple comparison test correction where significance was defined as p-value < 0.05. For comparison of *DR5pro::GFP* levels, WT and *crn* IM values were compared statistically using an unpaired t-test, where the p-value = 0.0007. Sample size (n) for all analyses can be found with each figure in the legend and refers to the number of individual plants analyzed.

Supplementary Material

Refer to Web version on PubMed Central for supplementary material.

ACKNOWLEDGEMNTS

We thank Yunde Zhao, the ABRC stock center, Paul Tarr, Joe Kieber, and Elena Shpak for sharing seeds, vectors, and reporter lines. We thank Tony D. Perdue, director of the UNC Biology Microscopy Core, for assistance with imaging. We thank Jamie Winshell and James Garzoni for lab and plant growth facility support. We thank UNC's High-Throughput Sequencing Facility for sequencing services. We thank members of the Nimchuk lab for critical

feedback on this project. This research was supported by a NIGMS-MIRA award from National Institutes of Health (R35GM119614) and the National Science Foundation (NSF) Plant Genome Research Program (PGRP; IOS-1546837) to Z.L.N. D.S.J. is supported by an NSF Postdoctoral Research Fellowship in Biology through the PGRP (NSF# 1906389).

References

1. Hallgrimsson B, Green RM, Katz DC, Fish JL, Bernier FP, Roseman CC, Young NM, Cheverud JM, and Marcucio RS (2019). The developmental-genetics of canalization In Seminars in cell & developmental biology, Volume 88 (Elsevier), pp. 67–79. [PubMed: 29782925]
2. Bradley D, Ratcliffe O, Vincent C, Carpenter R, and Coen E (1997). Inflorescence commitment and architecture in Arabidopsis. Science 275, 80–83. [PubMed: 8974397]
3. Reinhardt D, Mandel T, and Kuhlemeier C (2000). Auxin regulates the initiation and radial position of plant lateral organs. The Plant Cell 12, 507–518. [PubMed: 10760240]
4. Benková E, Michniewicz M, Sauer M, Teichmann T, Seifertová D, Jürgens G, and Friml J (2003). Local, efflux-dependent auxin gradients as a common module for plant organ formation. Cell 115, 591–602. [PubMed: 14651850]
5. Heisler MG, Ohno C, Das P, Sieber P, Reddy GV, Long JA, and Meyerowitz EM (2005). Patterns of auxin transport and gene expression during primordium development revealed by live imaging of the Arabidopsis inflorescence meristem. Current biology 15, 1899–1911. [PubMed: 16271866]
6. Yamaguchi N, Wu M-F, Winter CM, Berns MC, Nole-Wilson S, Yamaguchi A, Coupland G, Krizek BA, and Wagner D (2013). A molecular framework for auxin-mediated initiation of flower primordia. Developmental cell 24, 271–282. [PubMed: 23375585]
7. Weigel D (2012). Natural variation in Arabidopsis: from molecular genetics to ecological genomics. Plant physiology 158, 2–22. [PubMed: 22147517]
8. Somssich M, Je BI, Simon R, and Jackson D (2016). CLAVATA-WUSCHEL signaling in the shoot meristem. Development 143, 3238–3248. [PubMed: 27624829]
9. Pierre-Jerome E, Drapek C, and Benfey PN (2018). Regulation of division and differentiation of plant stem cells. Annual review of cell and developmental biology 34, 289–310.
10. Weigel D, Alvarez J, Smyth DR, Yanofsky MF, and Meyerowitz EM (1992). LEAFY controls floral meristem identity in Arabidopsis. Cell 69, 843–859. [PubMed: 1350515]
11. Pidkowich MS, Klenz JE, and Haughn GW (1999). The making of a flower: control of floral meristem identity in Arabidopsis. Trends in plant science 4, 64–70. [PubMed: 10234275]
12. Clark SE, Running MP, and Meyerowitz EM (1995). CLAVATA3 is a specific regulator of shoot and floral meristem development affecting the same processes as CLAVATA1. Development 121, 2057–2067.
13. Rodriguez-Leal D, Xu C, Kwon C-T, Soyars C, Demesa-Arevalo E, Man J, Liu L, Lemmon ZH, Jones DS, and Van Eck J (2019). Evolution of buffering in a genetic circuit controlling plant stem cell proliferation. Nature genetics 51, 786–792. [PubMed: 30988512]
14. Soyars CL, James SR, and Nimchuk ZL (2016). Ready, aim, shoot: stem cell regulation of the shoot apical meristem. Current opinion in plant biology 29, 163–168. [PubMed: 26803586]
15. Mayer KF, Schoof H, Haecker A, Lenhard M, Jurgens G, and Laux T (1998). Role of WUSCHEL in regulating stem cell fate in the Arabidopsis shoot meristem. Cell 95, 805–815. [PubMed: 9865698]
16. Jeong S, Trotochaud AE, and Clark SE (1999). The Arabidopsis CLAVATA2 gene encodes a receptor-like protein required for the stability of the CLAVATA1 receptor-like kinase. The Plant Cell 11, 1925–1933. [PubMed: 10521522]
17. Müller R, Bleckmann A, and Simon R (2008). The receptor kinase CORYNE of Arabidopsis transmits the stem cell-limiting signal CLAVATA3 independently of CLAVATA1. The Plant Cell 20, 934–946. [PubMed: 18381924]
18. Bleckmann A, Weidtkamp-Peters S, Seidel CA, and Simon R (2010). Stem cell signaling in Arabidopsis requires CRN to localize CLV2 to the plasma membrane. Plant physiology 152, 166–176. [PubMed: 19933383]

19. Nimchuk ZL, Tarr PT, and Meyerowitz EM (2011). An evolutionarily conserved pseudokinase mediates stem cell production in plants. The Plant Cell 23, 851–854. [PubMed: 21398569]
20. Nimchuk ZL (2017). CLAVATA1 controls distinct signaling outputs that buffer shoot stem cell proliferation through a two-step transcriptional compensation loop. PLoS genetics 13.
21. Wang G, Ellendorff U, Kemp B, Mansfield JW, Forsyth A, Mitchell K, Bastas K, Liu C-M, Woods-Tör A, and Zipfel C (2008). A genome-wide functional investigation into the roles of receptor-like proteins in Arabidopsis. Plant physiology 147, 503–517. [PubMed: 18434605]
22. Smyth DR, Bowman JL, and Meyerowitz EM (1990). Early flower development in Arabidopsis. The Plant Cell 2, 755–767. [PubMed: 2152125]
23. Reddy GV, Heisler MG, Ehrhardt DW, and Meyerowitz EM (2004). Real-time lineage analysis reveals oriented cell divisions associated with morphogenesis at the shoot apex of Arabidopsis thaliana. Development 131, 4225–4237. [PubMed: 15280208]
24. Long J, and Barton MK (2000). Initiation of axillary and floral meristems in Arabidopsis. Developmental biology 218, 341–353. [PubMed: 10656774]
25. Kayes JM, and Clark SE (1998). CLAVATA2, a regulator of meristem and organ development in Arabidopsis. Development 125, 3843–3851. [PubMed: 9729492]
26. Rédei J (1992). A note on Columbia wild type and Landsberg erecta. Methods in Arabidopsis Research 3.
27. Schultz EA, and Haughn GW (1991). LEAFY, a homeotic gene that regulates inflorescence development in Arabidopsis. The Plant Cell 3, 771–781. [PubMed: 12324613]
28. Clark SE, Williams RW, and Meyerowitz EM (1997). The CLAVATA1gene encodes a putative receptor kinase that controls shoot and floral meristem size in Arabidopsis. Cell 89, 575–585. [PubMed: 9160749]
29. DeYoung BJ, Bickle KL, Schrage KJ, Muskett P, Patel K, and Clark SE (2006). The CLAVATA1-related BAM1, BAM2 and BAM3 receptor kinase-like proteins are required for meristem function in Arabidopsis. The Plant Journal 45, 1–16. [PubMed: 16367950]
30. Nimchuk ZL, Zhou Y, Tarr PT, Peterson BA, and Meyerowitz EM (2015). Plant stem cell maintenance by transcriptional cross-regulation of related receptor kinases. Development 142, 1043–1049. [PubMed: 25758219]
31. Hu C, Zhu Y, Cui Y, Cheng K, Liang W, Wei Z, Zhu M, Yin H, Zeng L, and Xiao Y (2018). A group of receptor kinases are essential for CLAVATA signalling to maintain stem cell homeostasis. Nature plants 4, 205–211. [PubMed: 29581511]
32. Song S-K, Lee MM, and Clark SE (2006). POL and PLL1 phosphatases are CLAVATA1 signaling intermediates required for Arabidopsis shoot and floral stem cells. Development 133, 4691–4698. [PubMed: 17079273]
33. Goad DM, Zhu C, and Kellogg EA (2017). Comprehensive identification and clustering of CLV3/ESR-related (CLE) genes in plants finds groups with potentially shared function. New Phytologist 216, 605–616.
34. Fletcher JC, Brand U, Running MP, Simon R, and Meyerowitz EM (1999). Signaling of cell fate decisions by CLAVATA3 in Arabidopsis shoot meristems. Science 283, 1911–1914. [PubMed: 10082464]
35. Ogawa M, Shinohara H, Sakagami Y, and Matsubayashi Y (2008). Arabidopsis CLV3 peptide directly binds CLV1 ectodomain. Science 319, 294–294. [PubMed: 18202283]
36. Lachowiec J, Queitsch C, and Kliebenstein DJ (2016). Molecular mechanisms governing differential robustness of development and environmental responses in plants. Annals of botany 117, 795–809. [PubMed: 26473020]
37. Alonso-Blanco C, El-Assal SE-D, Coupland G, and Koornneef M (1998). Analysis of natural allelic variation at flowering time loci in the Landsberg erecta and Cape Verde Islands ecotypes of Arabidopsis thaliana. Genetics 149, 749–764. [PubMed: 9611189]
38. Gray WM, Östin A, Sandberg G, Romano CP, and Estelle M (1998). High temperature promotes auxin-mediated hypocotyl elongation in Arabidopsis. Proceedings of the National Academy of Sciences 95, 7197–7202.
39. Quint M, Delker C, Franklin KA, Wigge PA, Halliday KJ, and van Zanten M (2016). Molecular and genetic control of plant thermomorphogenesis. Nature plants 2, 1–9.

40. Franklin KA, Lee SH, Patel D, Kumar SV, Spartz AK, Gu C, Ye S, Yu P, Breen G, and Cohen JD (2011). Phytochrome-interacting factor 4 (PIF4) regulates auxin biosynthesis at high temperature. Proceedings of the National Academy of Sciences 108, 20231–20235.
41. Sun J, Qi L, Li Y, Chu J, and Li C (2012). PIF4-mediated activation of YUCCA8 expression integrates temperature into the auxin pathway in regulating Arabidopsis hypocotyl growth. PLoS genetics 8.
42. Box MS, Huang BE, Domijan M, Jaeger KE, Khattak AK, Yoo SJ, Sedivy EL, Jones DM, Hearn TJ, and Webb AA (2015). ELF3 controls thermoresponsive growth in Arabidopsis. Current biology 25, 194–199. [PubMed: 25557663]
43. Ashburner M, Ball CA, Blake JA, Botstein D, Butler H, Cherry JM, Davis AP, Dolinski K, Dwight SS, and Eppig JT (2000). Gene ontology: tool for the unification of biology. Nature genetics 25, 25–29. [PubMed: 10802651]
44. Consortium GO (2019). The gene ontology resource: 20 years and still GOing strong. Nucleic acids research 47, D330–D338. [PubMed: 30395331]
45. Mi H, Muruganujan A, Huang X, Ebert D, Mills C, Guo X, and Thomas PD (2019). Protocol Update for large-scale genome and gene function analysis with the PANTHER classification system (v. 14.0). Nature protocols 14, 703–721. [PubMed: 30804569]
46. Sabatini S, Beis D, Wolkenfelt H, Murfett J, Guilfoyle T, Malamy J, Benfey P, Leyser O, Bechtold N, and Weisbeek P (1999). An auxin-dependent distal organizer of pattern and polarity in the Arabidopsis root. Cell 99, 463–472. [PubMed: 10589675]
47. Friml J, Vieten A, Sauer M, Weijers D, Schwarz H, Hamann T, Offringa R, and Jürgens G (2003). Efflux-dependent auxin gradients establish the apical-basal axis of Arabidopsis. Nature 426, 147–153. [PubMed: 14614497]
48. Cheng Y, Dai X, and Zhao Y (2006). Auxin biosynthesis by the YUCCA flavin monooxygenases controls the formation of floral organs and vascular tissues in Arabidopsis. Genes & development 20, 1790–1799. [PubMed: 16818609]
49. Krizek B (2009). AINTEGUMENTA and AINTEGUMENTA-LIKE6 act redundantly to regulate Arabidopsis floral growth and patterning. Plant physiology 150, 1916–1929. [PubMed: 19542297]
50. Prigge MJ, Platre M, Kadakia N, Zhang Y, Greenham K, Szutu W, Pandey BK, Bhosale RA, Bennett MJ, and Busch W (2020). Genetic analysis of the Arabidopsis TIR1/AFB auxin receptors reveals both overlapping and specialized functions. Elife 9.
51. Mashiguchi K, Tanaka K, Sakai T, Sugawara S, Kawaide H, Natsume M, Hanada A, Yaeno T, Shirasu K, and Yao H (2011). The main auxin biosynthesis pathway in Arabidopsis. Proceedings of the National Academy of Sciences 108, 18512–18517.
52. Won C, Shen X, Mashiguchi K, Zheng Z, Dai X, Cheng Y, Kasahara H, Kamiya Y, Chory J, and Zhao Y (2011). Conversion of tryptophan to indole-3-acetic acid by TRYPTOPHAN AMINOTRANSFERASES OF ARABIDOPSIS and YUCCAs in Arabidopsis. Proceedings of the National Academy of Sciences 108, 18518–18523.
53. Lavy M, and Estelle M (2016). Mechanisms of auxin signaling. Development 143, 3226–3229. [PubMed: 27624827]
54. Björkman T, and Pearson KJ (1998). High temperature arrest of inflorescence development in broccoli (Brassica oleracea var. italica L.). Journal of Experimental Botany 49, 101–106.
55. Anderson R, Bayer PE, and Edwards D (2020). Climate change and the need for agricultural adaptation. Current Opinion in Plant Biology.
56. Torii KU, Mitsukawa N, Oosumi T, Matsuura Y, Yokoyama R, Whittier RF, and Komeda Y (1996). The Arabidopsis ERECTA gene encodes a putative receptor protein kinase with extracellular leucine-rich repeats. The Plant Cell 8, 735–746. [PubMed: 8624444]
57. Kinoshita A, Betsuyaku S, Osakabe Y, Mizuno S, Nagawa S, Stahl Y, Simon R, Yamaguchi-Shinozaki K, Fukuda H, and Sawa S (2010). RPK2 is an essential receptor-like kinase that transmits the CLV3 signal in Arabidopsis. Development 137, 3911–3920. [PubMed: 20978082]
58. Lita PY, Miller AK, and Clark SE (2003). POLTERGEIST encodes a protein phosphatase 2C that regulates CLAVATA pathways controlling stem cell identity at Arabidopsis shoot and flower meristems. Current Biology 13, 179–188. [PubMed: 12573213]

59. Hicks KA, Millar AJ, Carre IA, Somers DE, Straume M, Meeks-Wagner DR, and Kay SA (1996). Conditional circadian dysfunction of the Arabidopsis early-flowering 3 mutant. Science 274, 790–792. [PubMed: 8864121]
60. Hazak O, Brandt B, Cattaneo P, Santiago J, Rodriguez-Villalon A, Hothorn M, and Hardtke CS (2017). Perception of root-active CLE peptides requires CORYNE function in the phloem vasculature. EMBO reports 18, 1367–1381. [PubMed: 28607033]
61. Blilou I, Xu J, Wildwater M, Willemsen V, Paponov I, Friml J, Heidstra R, Aida M, Palme K, and Scheres B (2005). The PIN auxin efflux facilitator network controls growth and patterning in Arabidopsis roots. Nature 433, 39–44. [PubMed: 15635403]
62. Zhang W, To JP, Cheng CY, Eric Schaller G, and Kieber JJ (2011). Type-A response regulators are required for proper root apical meristem function through post-transcriptional regulation of PIN auxin efflux carriers. The Plant Journal 68, 1–10. [PubMed: 21645147]
63. Vernoux T, Brunoud G, Farcot E, Morin V, Van den Daele H, Legrand J, Oliva M, Das P, Larrieu A, and Wells D (2011). The auxin signalling network translates dynamic input into robust patterning at the shoot apex. Molecular systems biology 7, 508. [PubMed: 21734647]
64. Wiśniewska J, Xu J, Seifertová D, Brewer PB, Růžička K, Blilou I, Rouquié D, Benková E, Scheres B, and Friml J (2006). Polar PIN localization directs auxin flow in plants. Science 312, 883–883. [PubMed: 16601151]
65. Peterson BA, Haak DC, Nishimura MT, Teixeira PJ, James SR, Dangl JL, and Nimchuk ZL (2016). Genome-wide assessment of efficiency and specificity in CRISPR/Cas9 mediated multiple site targeting in Arabidopsis. PloS one 11.
66. LeBlanc C, Zhang F, Mendez J, Lozano Y, Chatpar K, Irish VF, and Jacob Y (2018). Increased efficiency of targeted mutagenesis by CRISPR/Cas9 in plants using heat stress. The Plant Journal 93, 377–386. [PubMed: 29161464]
67. Hodgens C, Nimchuk ZL, and Kieber JJ (2017). indCAPS: A tool for designing screening primers for CRISPR/Cas9 mutagenesis events. PloS one 12.
68. Clough SJ, and Bent AF (1998). Floral dip: a simplified method for Agrobacterium-mediated transformation of Arabidopsis thaliana. The plant journal 16, 735–743. [PubMed: 10069079]
69. Ishihara H, Sugimoto K, Tarr PT, Temman H, Kadokura S, Inui Y, Sakamoto T, Sasaki T, Aida M, and Suzuki T (2019). Primed histone demethylation regulates shoot regenerative competency. Nature communications 10, 1–15.
70. Prunet N, Jack TP, and Meyerowitz EM (2016). Live confocal imaging of Arabidopsis flower buds. Developmental biology 419, 114–120. [PubMed: 26992363]
71. Nimchuk ZL, and Perdue TD (2017). Live imaging of shoot meristems on an inverted confocal microscope using an objective lens inverter attachment. Frontiers in plant science 8, 773. [PubMed: 28579995]
72. Schindelin J, Arganda-Carreras I, Frise E, Kaynig V, Longair M, Pietzsch T, Preibisch S, Rueden C, Saalfeld S, and Schmid B (2012). Fiji: an open-source platform for biological-image analysis. Nature methods 9, 676–682. [PubMed: 22743772]
73. Pertea M, Kim D, Pertea GM, Leek JT, and Salzberg SL (2016). Transcript-level expression analysis of RNA-seq experiments with HISAT, StringTie and Ballgown. Nat Protoc 11, 1650–1667. [PubMed: 27560171]
74. Liao Y, Smyth GK, and Shi W (2013). The Subread aligner: fast, accurate and scalable read mapping by seed-and-vote. Nucleic acids research 41, e108–e108. [PubMed: 23558742]
75. Risso D, Schwartz K, Sherlock G, and Dudoit S (2011). GC-Content Normalization for RNA-Seq Data. BMC Bioinformatics 12, 480. [PubMed: 22177264]
76. Risso D, Ngai J, Speed TP, and Dudoit S (2014). Normalization of RNA-seq data using factor analysis of control genes or samples. Nature biotechnology 32, 896–902.
77. Robinson MD, McCarthy DJ, and Smyth GK (2010). edgeR: a Bioconductor package for differential expression analysis of digital gene expression data. Bioinformatics 26, 139–140. [PubMed: 19910308]
78. Thomas PD, Campbell MJ, Kejariwal A, Mi H, Karlak B, Daverman R, Diemer K, Muruganujan A, and Narechania A (2003). PANTHER: A Library of Protein Families and Subfamilies Indexed by Function. Genome Research 13, 2129–2141. [PubMed: 12952881]

79. Bray NL, Pimentel H, Melsted P, and Pachter L (2016). Near-optimal probabilistic RNA-seq quantification. Nature Biotechnology 34, 525–527.

80. Pimentel H, Bray NL, Puente S, Melsted P, and Pachter L (2017). Differential analysis of RNA-seq incorporating quantification uncertainty. Nature methods 14, 687–690. [PubMed: 28581496]

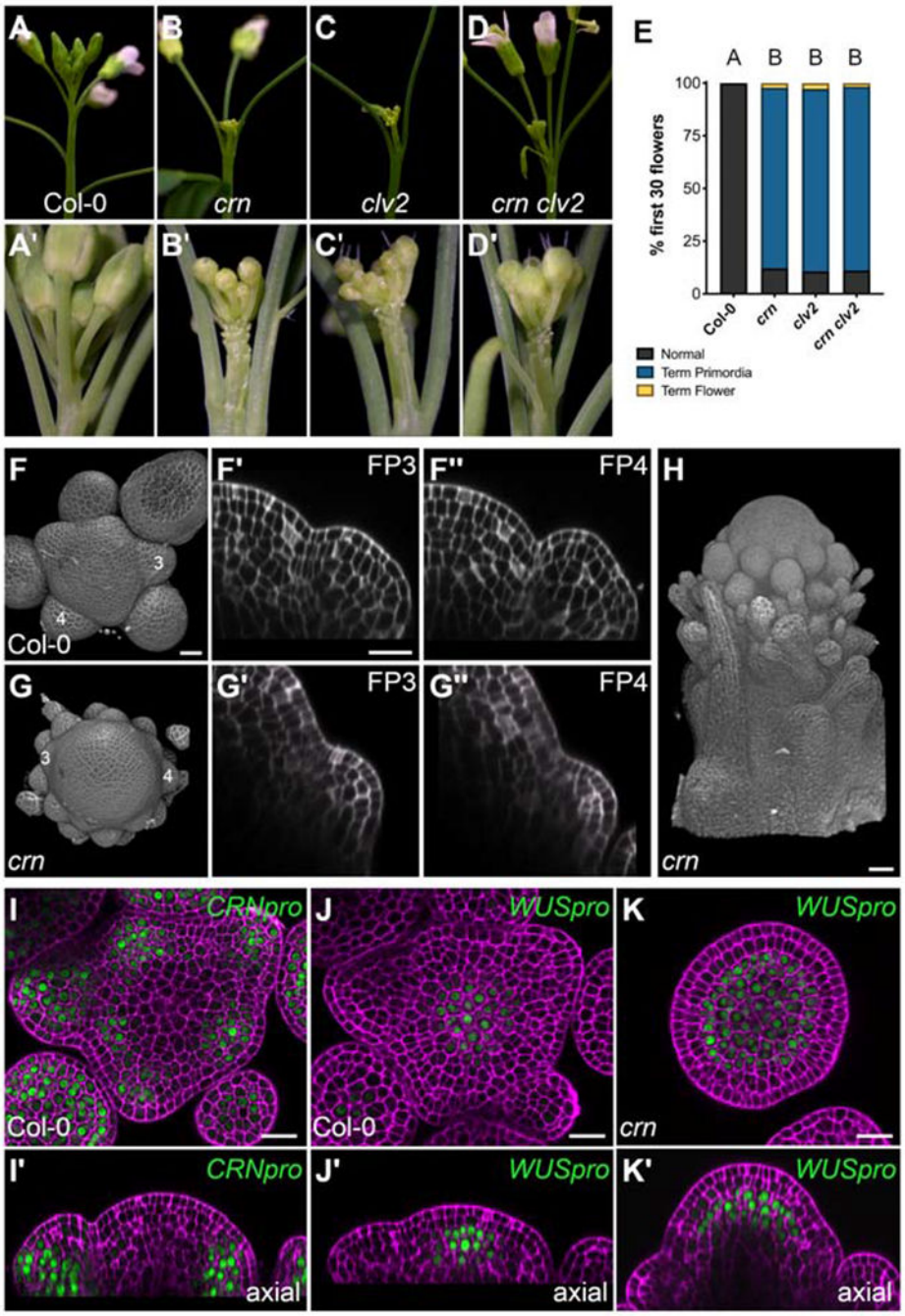

Figure 1. Flower primordia outgrowth is disrupted in *clv2/crn*

(A-D) Inflorescences of Col-0, *crn* (*crn-10*), *clv2* (*rlp10-1*), and *crn clv2* double mutants.

(A'-D') Close up showing flower primordia termination in *crn, clv2* and *crn clv2*.

(E) Quantification of flower termination, classifying the first 30 attempts to make a flower as: normal (grey), terminated primordia (blue) or terminated flowers (yellow) in Col-0 (n=28), *crn* (n=27), *clv2* (n=25), and *crn clv2* (n=25).

(F and G) 3-D reconstruction of inflorescence meristems of (F) Col-0 (n=4) and (G) crn (n=6). Axial view of the (F', G') third (FP3) and (F", G") fourth (FP4) flower primordia

(labeled 3 and 4 in (F) and (G)) revealing developmental differences. FP3 and FP4 were determined by identifying the 3rd and 4th earliest detectable primordia along the IM, respectively. Staging similar to [23].

(H) Side view of a young inflorescence meristem of *crn* during the termination phase (n=5).

(I-K) Expression patterns of *YPET-N7* reporter lines in the IM with XY view of L5 layer (I-K) and axial view (Z-axis) of same IM stack (I'-K') shown for each: (I) *CRNpro* in Col-0 (n=6), (J) *WUSpro* in Col-0 (n=6), (K) *WUSpro* in *crn* (n=6). Tissue stained with propidium iodide (PI; magenta).

Statistical groupings based on significant differences found using Kruskal-Wallis and Dunn's multiple comparison test correction (E). Scale bars, 50μm in (H), 20μm in (F-G) and (I-K).

See also Figure S1, Figure S4, and Video S1.

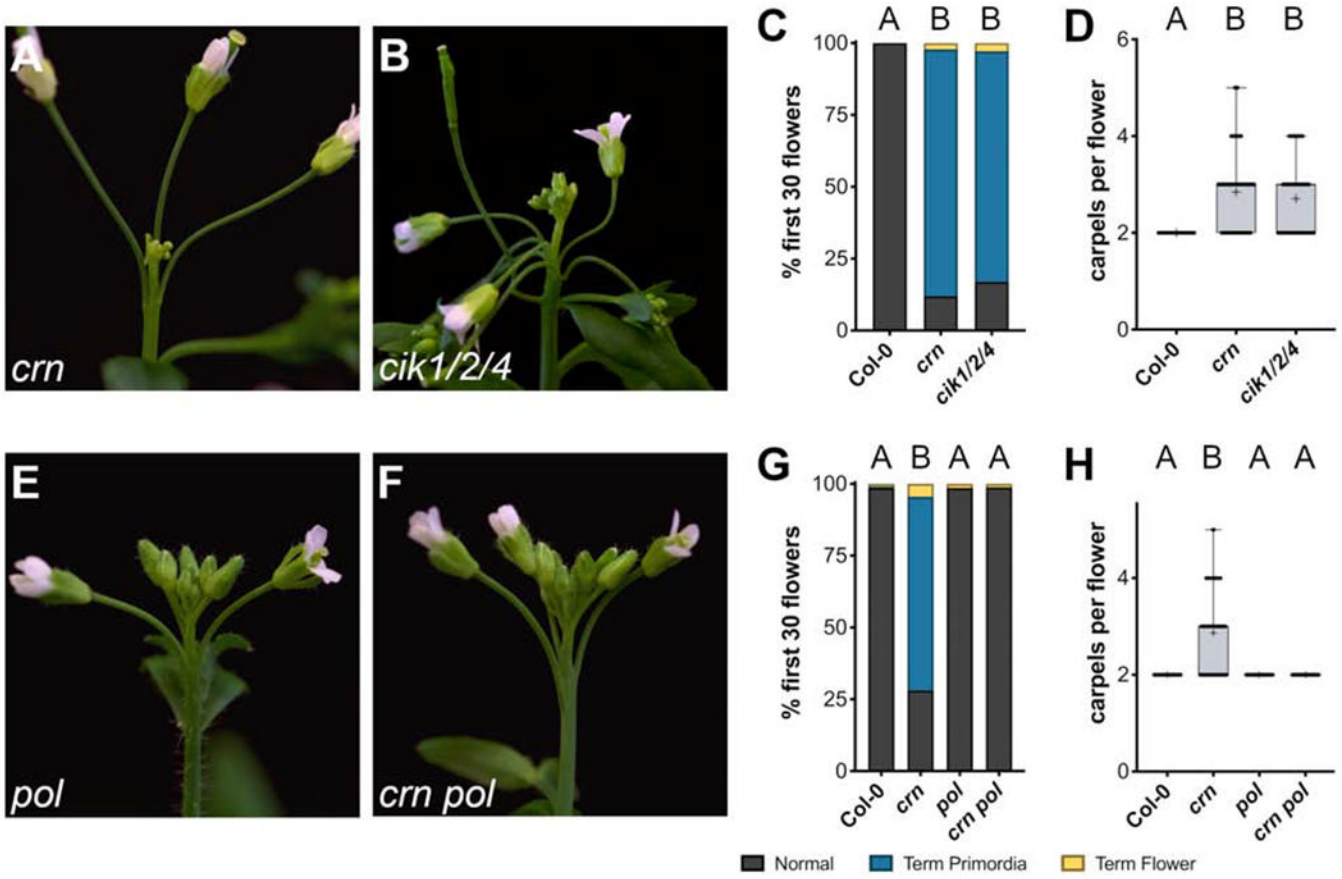

Figure 2. CLV2/CRN-mediated flower outgrowth requires CIK1/2/4 co-receptors and a downstream *POL*-dependent pathway

(A-B) Inflorescence of *crn* and *cik1/2/4* (*cik1-3/cik2-3/cik4-3*) mutant plants reveal similar flower termination defects. Quantification of (C) flower termination and (D) carpel number across Col-0 (n=16), *crn* (n=17), and *cik1/2/4* (n=13).

(E-F) Inflorescence of *crn* and *crn pol* showing that flower termination is suppressed by *pol* (*pol-6*). Quantification of (G) flower termination and (H) carpel number across Col-0 (n=15), *crn* (n=15), *pol* (n=15), and *crn pol* (n=14).

Box and whisker plots show full range of data (min to max) with mean marked as "+". Statistical groupings based on significant differences found using Kruskal-Wallis and Dunn's multiple comparison test correction (C-D and G-H).

See also Figure S2.

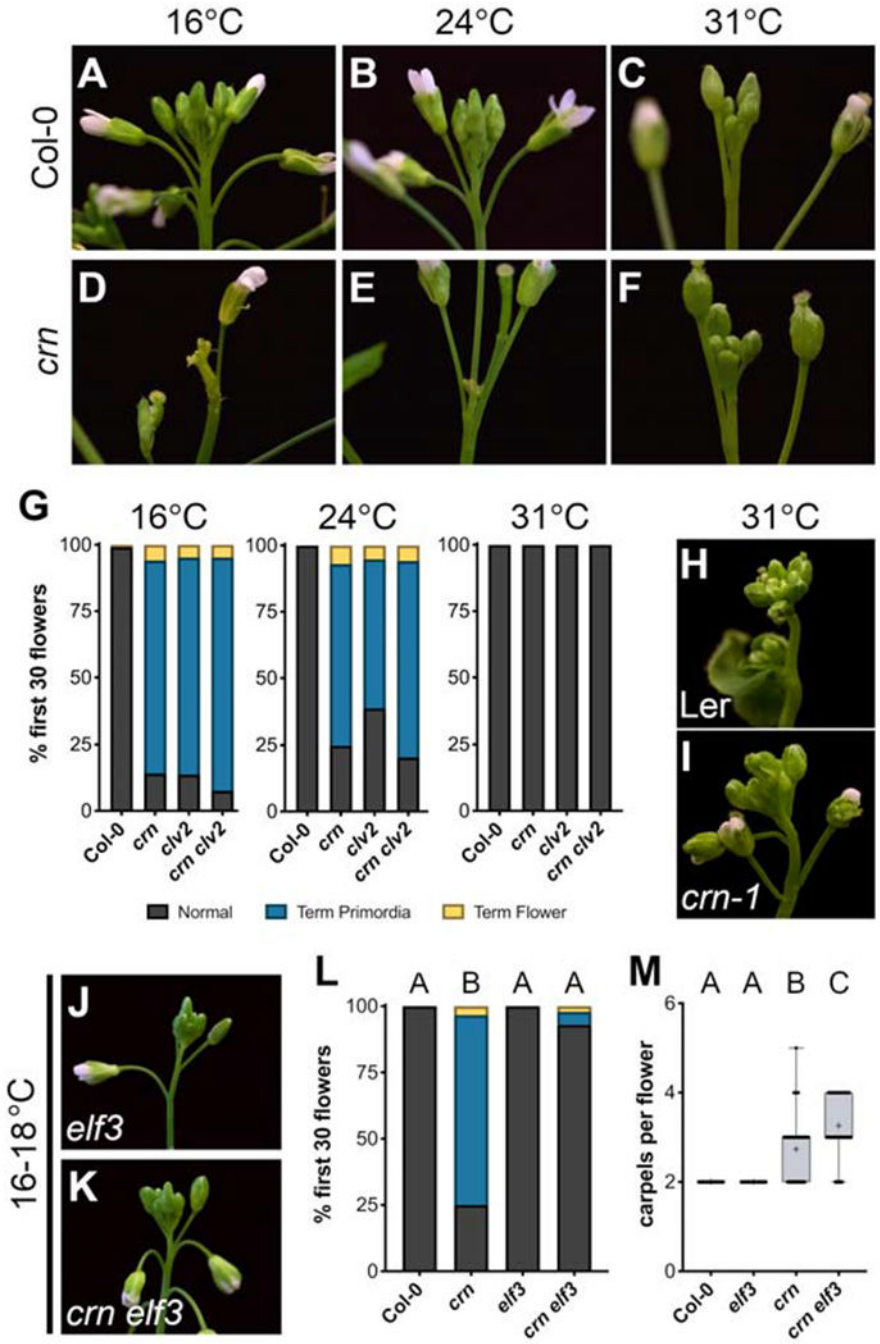

Figure 3. High temperature responses modulate *clv2/crn* flower primordia outgrowth

(A-F) Temperature-dependent inflorescence phenotypes of *crn* compared to Col-0. Flower primordia termination in *crn* is prevalent at (D) 16°C and (E) 24°C, but is suppressed at (F) 31°C.

(G) Quantification of flower primordia termination at 16°C: Col-0 (n=8), *crn* (n=9), *clv2* (n=9), *crn clv2* (n=7), 24°C: Col-0 (n=9), *crn* (n=9), *clv2* (n=9), *crn clv2* (n=9), and 31°C: Col-0 (n=8), *crn* (n=9), *clv2* (n=9), *crn clv2* (n=6).

(H-I) Inflorescences of Ler and *crn-1* grown at 31°C.

(J-K) Inflorescences of *elf3* (*elf3-1*) and *crn elf3* grown at 16-18°C
(L-M) Quantification of (L) flower primordia termination and (M) carpel number in Col-0 (n=24), *crn* (n=18), *elf3* (n=27), *crn elf3* (n=26) grown at 16-18°C.
Box and whisker plots show full range of data (min to max) with mean marked as "+". Statistical groupings based on significant differences found using Kruskal-Wallis and Dunn's multiple comparison test correction (L-M).
See also Figure S4.

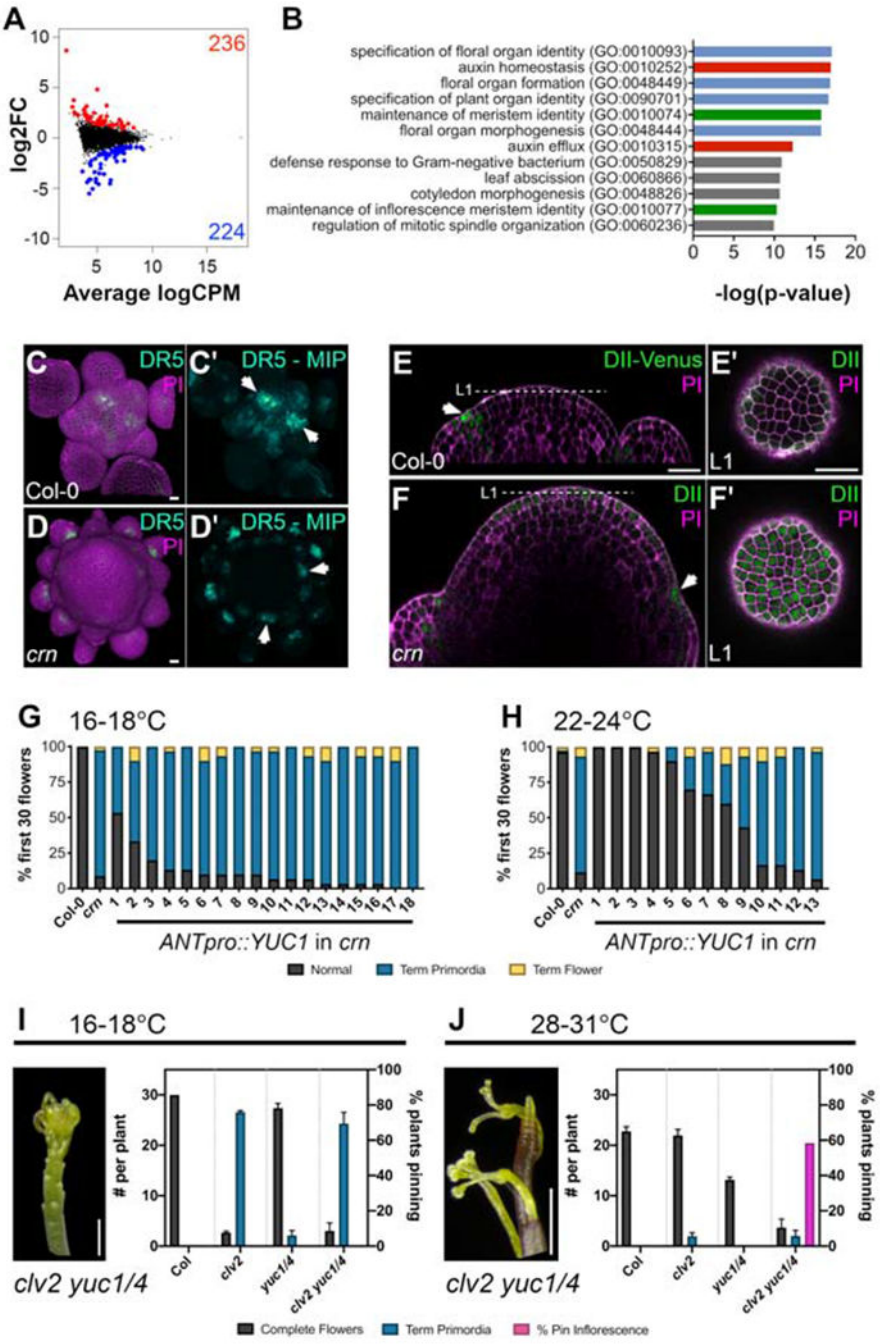

Figure 4. Flower primordia outgrowth is maintained by separable auxin-dependent processes in different thermal conditions

(A) Differentially expressed genes (DEG, p-value < 0.001) between *crn* and WT IMs; upregulated genes (red), downregulated genes (blue).

(B) Top GO terms enriched in *crn* DEGs, highlighting terms associated with flower development (blue), meristem maintenance (green) and auxin (red).

(C-D) Maximum intensity projection (MIP) of *DR5::GFP* (teal) in the IM of (C) Col-0 (n=14) and (D) *crn* (n=12). Stained with PI (magenta). Arrows point to primordia used for DR5 quantification/comparison.

(E-F) Axial view showing DII-Venus (green) expression pattern in (E) Col-0 (n=6) and (F) *crn* (n=8) IMs. Stained with PI (magenta). (E'-F') L1 layer of IMs from (E') Col-0 and (F') *crn* used to quantify percent of L1 cells with DII marker. Arrows point to organ boundaries where DII reporter can be detected in the L1 of Col-0 and *crn*.

(G-H) Flower primordia termination across independent T1 lines of *ANTpro::YUC1* in *crn* compared to Col-0 and *crn* when grown at (G) 16-18°C or (H) 22-24°C.

(I) *clv2 yuc1/4* inflorescence grown at colder temperatures (16-18°C) and quantification of flower outgrowth defects in Col-0 (n=9), *clv2* (n=9), *yuc1/4* (n=8), *clv2 yuc1/4* (n=10).

(J) *clv2 yuc1/4* pin-like inflorescence grown at hot temperatures (28-31°C) and quantification of flower outgrowth defects, including instances of pins (pink bar; right y-axis) in Col-0 (n=29), *clv2* (n=20), *yuc1/4* (n=20), *clv2 yuc1/4* (n=12).

Scale bars, 20μm in (C-D) and (E-F), 1mm in (I-J).

Bar plots show mean with SEM.

See also Figures S3 and S4, Tables S1–S3.

KEY RESOURCES TABLE

REAGENT or RESOURCE	SOURCE	IDENTIFIER
Bacterial and Virus Strains		
E. coli strain DH5α	Widely distributed	N/A
E. coli strain DB3.1	Widely distributed	N/A
Agrobacterium tumefaciens strain GV3101	Widely distributed	N/A
Chemicals, Peptides, and Recombinant Proteins		
Propidium Iodide (PI)	Thermo Fisher	Cat#P1304MP
Murashige and Skoog (MS) Basal Salt Micronutrient Solution	Sigma-Aldrich	Cat#M0529
Methyl Salicylate	Sigma-Aldrich	Cat#M6752
Critical Commercial Assays		
Gateway LR Clonase II Enzyme mix	Thermo Fisher	Cat#11791020
Gateway BP Clonase II Enzyme mix	Thermo Fisher	Cat#11789020
pENTR/D-TOPO Cloning Kit	Thermo Fisher	Cat#K240020
Golden Gate Assembly Mix	NEB	Ca#E1601S
EZNA Plant RNA Kit	Omega Bio-tek	SKU:R6827-01
RNase-free DNase	Omega Bio-tek	SKU:E1091-02
Stranded mRNA-seq Kit	Kapa Biosystems	Cat#07962169001
Deposited Data		
Raw RNAseq data	This paper	SRA BioProject: PRJNA66106
Code to analyze RNAseq data	This paper	https://github.com/NimchukLab
Arabidopsis thaliana TAIR10.1 reference genome	The Arabidopsis Information Resource (TAIR)	SRA BioSample: SAMN03081427
Arabidopsis thaliana TAIR10 Transcriptome	EnsemblPlants	https://plants.ensembl.org/Arabidopsis_thaliana/Info/Index
Experimental Models: Organisms/Strains		
Arabidopsis thaliana: Col-0 ecotype	N/A	N/A
Arabidopsis: crn-10	[20]	N/A
Arabidopsis: rlp10-1	[20]	GABI_686A09
Arabidopsis: er-105	[56]	N/A
Arabidopsis: lfy-1	[27]	ABRC CS6228
Arabidopsis: clv3-9	[30]	N/A
Arabidopsis: dodeca-cle	[13]	N/A

REAGENT or RESOURCE	SOURCE	IDENTIFIER
Arabidopsis: clv1-101	[57]	N/A
Arabidopsis: bam1-4	[30]	N/A
Arabidopsis: bam2-4	[30]	N/A
Arabidopsis: bam3-2	[30]	N/A
Arabidopsis: pol-6	[58]	N/A
Arabidopsis: elf3-1	[59]	ABRC CS3787
Arabidopsis: yuc1	[48]	SALK_106293
Arabidopsis: yuc4	[48]	SM_3_16128
Arabidopsis thaliana: Landsberg *erecta (Ler)* ecotype	N/A	N/A
Arabidopsis: crn-1 (Ler)	[17]	ABRC CS9853
Arabidopsis: clv2-1 (Ler)	[16]	N/A
Arabidopsis: crn CRNpro::CRN-GFP	[20]	N/A
Arabidopsis: clv2 CLV2pro::CLV2-CITRINE	[60]	N/A
Arabidopsis: Col-0 *WUSp:YN7*	gift from Paul Tarr - Caltech	N/A
Arabidopsis: Col-0 *DR5-GFP*	[61–62]	N/A
Arabidopsis: Col-0 *DII-Venus*	[63]	N/A
Arabidopsis: Col-0 *PIN1pro::PIN1-GFP*	[64]	N/A
Arabidopsis: crn WUSp:YN7	This study	N/A
Arabidopsis: cik1-3	This study	N/A
Arabidopsis: cik2-3	This study	N/A
Arabidopsis: cik4-3	This study	N/A
Arabidopsis: clv2-10 (Ler)	This study	N/A
Arabidopsis: clv2-11 (Ler)	This study	N/A
Oligonucleotides		
cik1 BslI dCAPS F	dCAPs primer for cik1 genotyping	CTGGTTTTTGTATGGTTCTTTGATATCTCTTCTGCTACACTTCCTC
cik1 BslI dCAPS R	dCAPs primer for cik1 genotyping	GATAAATTCATAGAGAAAAAAATTGAGATTTCTCC
cik2 BslI dCAPS F	dCAPs primer for cik2 genotyping	CATCTTTGTTTTGTTTTTTCCCCCTTCCAGAG
cik2 BslI dCAPS R	dCAPs primer for cik2 genotyping	CAAACAAAATAATCTTACACTTGTCGAAG
cik4 BslI dCAPS F	dCAPs primer for cik4 genotyping	AACAAGATGAAAGATGAGAAAGAGGCCTT
cik4 BslI dCAPS R	dCAPs primer for cik4 genotyping	CTCACAGAGAAACCACAAAACCTTC

REAGENT or RESOURCE	SOURCE	IDENTIFIER
ANT Pro F	AINTEGUMENTA promoter for pANTpro:GTW	GGGAGCTCGTCGAGCGGCCGAAATTGGAATTATTCATATTAATGAGTTAGC
ANT Pro R	AINTEGUMENTA promoter for pANTpro:GTW	CCCCGGGGGTTTCTTTTTTTGGTTTCTGCTTCTCTTCTTTC
YUC1 F	YUCCA1 CDS for entry vector	CACCAAAAAATGGAGTCTCATCCTCACAACAAAACTGACCAG
YUC1 R	YUCCA1 CDS for entry vector	TTAGGATTTAGAGGTAAAGACAAAACGAGAACTGCACATATTCC
Recombinant DNA		
Plasmid *ANTp:YUC1*	This study	N/A
Plasmid *CRNp:YN7*	This study	N/A
Plasmid *pENTR-GG*	This study	N/A
Software and Algorithms		
Fiji/ImageJ v.2.0.0-rc-69/1.52u	National Institutes of Health	https://imagej.net/Fiji
Zen Microscope Imaging Software	Zeiss	https://www.zeiss.com/
NIS-Elements Imaging Software	Nikon	https://www.microscope.healthcare.nikon.com/products/software
GIMP GNU image manipulation program 2.10.4	GIMP	https://www.gimp.org/
Lapse-it iOS 12.3.1	Apple app store	http://www.lapseit.com/
Prism v.8.3.2	GraphPad	https://www.graphpad.com/
indCAPS	[67]	http://indcaps.kieber.cloudapps.unc.edu/
HISAT2 2.2.0	[73]	https://github.com/DaehwanKimLab/hisat2
Subread 1.5.1	[74]	https://github.com/DeskGen/subread
EDASeq 2.22.0	[75]	https://github.com/drisso/EDASeq
RUVseq 1.22.0	[76]	https://github.com/drisso/RUVSeq
EdgeR 3.33.0	[77]	https://gist.github.com/jdblischak/11384914
Kallisto 0.44.0	[79]	https://github.com/pachterlab/kallisto
Sleuth 0.33.0	[80]	https://github.com/pachterlab/sleuth
GO term analysis Panther	[78]	http://geneontology.org/
Other		
Small glass-bottom petri dish	MatTek Corporation	Cat#P35G-1.5-10-C